A Numerical Study of Combustion Stability in Emergency Oxygen Generators

Victor Diakov, Evgeny Shafirovich, and Arvind Varma
School of Chemical Engineering, Purdue University, 480 Stadium Mall Drive, West Lafayette, IN 47907

DOI 10.1002/aic.10726
Published online November 10, 2005 in Wiley InterScience (www.interscience.wiley.com).

Combustion in sodium chlorate based emergency oxygen generators is accompanied by significant oscillations of the product oxygen flow rate, which decrease the efficiency of these devices. Reactant melting and convective heat transfer from the generated gas are key steps in the process. In this work, the effect of reactant melting on filtration combustion front propagation stability in gas generating mixtures is investigated numerically. The formation of melting regions is demonstrated in cases with significant convective gas-to-core heat transfer. Numerical simulations exhibit the oscillatory behavior of oxygen generation. By decreasing the effective heat of reaction, reactant melting is detrimental to combustion front stability. The simulations show growth of pulsations with increasing reaction activation energy and decreasing convective heat transfer. A strong stabilization of front propagation is observed when combustion temperature reaches the melting point of reaction product. These results identify the important factors responsible for pulsating behavior of chemical oxygen generators. © 2005 American Institute of Chemical Engineers *AIChE J,* 52: 1495–1501, 2006
Key words: emergency oxygen generators, combustion, gas generation, instability, oscillations

Introduction

As a part of the broader area of solid reactants combustion,[1] with applications ranging from rocket propellants and pyrotechnic mixtures to materials synthesis,[2,3] combustion front propagation for gas generation is an important topic which has attracted significant research effort.[4,5] In its simplest case, the traveling combustion wave includes a relatively thin reaction zone, also referred to as reaction sheet or *combustion front*, moving through a mixture of solid reactants. High reaction exothermicity enables the self-propagating nature of the process when coupled with heat transport in the form of thermal conduction, radiation, melted component flow or convective transfer between flowing gas and solid sample. The latter, referred to as *filtration combustion* (FC), has a number of significant applications, such as underground burning and smoldering, oil extraction and waste incineration.[6]

In FC, the gas may not only exchange heat, but also carry a reactant, for example, oxygen in the case of smoldering combustion. In this article, we consider a different case involving a combustion system for oxygen generation, where O_2 is not a reactant but the desired reaction product. Emergency oxygen generators typically contain $NaClO_3$ as the source of oxygen:

$$NaClO_3 \rightarrow NaCl + 3/2O_2, \quad (1)$$

metal fuel (Sn) to enhance the exothermic effect, catalyst (Co_3O_4) to promote sodium chlorate decomposition, and other minor ingredients. As shown in our recent experimental studies,[4,7] these devices exhibit significant (and undesirable) oscillations in the rate of oxygen generation, and the factors responsible for them remain unclear. One reason for this, not previously recognized, is that during the combustion process, the sample temperature rises to $\sim$ 750°C, well above the $NaClO_3$ melting point (255°C). In this study, we focus on the

Correspondence concerning this article should be addressed to A. Varma at avarma@purdue.edu.

effect of reactant melting on the stability of combustion front propagation for the case of filtration combustion, specifically as applied to emergency oxygen generators.

The widely accepted approach in studies of combustion front propagation stability involves two aspects. First, a steady-state solution representing the combustion front moving with a constant velocity is determined. For this, the approximation of an infinitely thin reaction zone is used, that is, it is assumed that the reaction occurs instantly, which greatly simplifies the analysis. Next, the evolution of small deviations from the steady-state solution is considered.

Following this approach, combustion front stability in heterogeneous systems was analyzed for gasless combustion with or without reactant melt spreading,[8,9] as well as for FC.[10] The typical assumptions in theoretical studies include the thin reaction zone approximation, small magnitude of perturbations, constant thermal conductivity and heat capacity, uniform reaction medium, and gas-to-solid heat transfer coefficient independent of gas flow velocity.

An interesting diversification from the above path has been developed in an effort to describe combustion in nonuniform media.[11-13] The authors use mapping to analyze the stability of localized reaction zones propagation. Numerical simulations have also been helpful in relaxing the earlier assumptions as, for example, Krishenik and Shkadinskii[14] have studied the influence of nonlinear variation of thermal conductivity with temperature on combustion front stability.

It is believed that further progress in the field of combustion theory will occur through computational modeling.[15] Various publications present numerical simulations of combustion front stability,[16] including systems with melting or other phase transitions.[8, 17-19] It is widely agreed that low-temperature reactant melting (or endothermic phase transition in a more general case) stimulates pulsations in combustion front propagation while, on the other hand, the high-temperature melting of reaction products stabilizes the combustion wave.

While reactant melting is a key step in sodium chlorate based oxygen generation, it has previously not been considered in FC models or computational studies. For this reason, in light of our experimental observations, in this work we numerically investigate the thermal effect of reactant melting on FC front propagation stability in gas generating mixtures.

Model Description

In developing the model, we incorporate experimental data on sample heat capacity, phase transition and reaction kinetics in the classic FC equations.[10] Note that in systems with melt spreading, unstable front propagation frequently leads to nonuniformly distributed reaction products in the sample.[8] Since this nonuniformity was not observed experimentally for oxygen generators, we account for only the thermal effect of melting. To describe the experimentally observed propagation of the combustion front along the sample, the following set of equations is used

$$\frac{\partial V}{\partial z} = \frac{3}{2} R(\eta, T) \tag{2}$$

$$C_{pg} \frac{\partial (V \cdot T_g)}{\partial z} = C_{pg} T \frac{\partial V}{\partial z} + \tilde{\alpha} S (T - T_g) \tag{3}$$

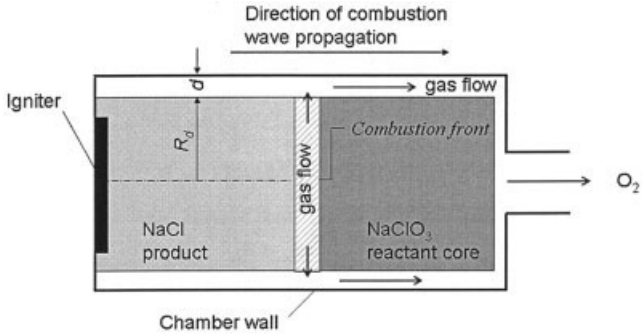

Figure 1. Emergency oxygen generator.

$$\rho_0 \frac{\partial \eta}{\partial t} = R(\eta, T) \tag{4}$$

$$\rho_0 \cdot C_p \frac{\partial T}{\partial t} = \frac{\partial \left(k \frac{\partial T}{\partial z} \right)}{\partial z} + (-\Delta H_r) R(\eta, T) - \tilde{\alpha} S (T - T_g) \tag{5}$$

$$R(\eta, T) = \rho_0 (1 - \eta) k_0 \exp\left(- \frac{E_a}{R_g T} \right) \tag{6}$$

The earlier expressions represent mass (2 and 4) and energy (3 and 5) balances for gaseous (2 and 3), and condensed (4 and 5) phases, respectively, and reaction kinetics (6). Since pressure is close to ambient, gas heat capacity in the generator is negligible and heat accumulation term is omitted from gas heat balance (3). The stoichiometric coefficient 3/2 for O_2 release from $NaClO_3$ is present in Eq. 2.

Since reactant melting is of key importance for the process under investigation, detailed experimental thermal analysis data were used to calculate species heat capacities and enthalpies as functions of temperature. Note that only in the ideal case of large crystals, melting occurs at a well defined temperature T_m, and the enthalpy of components can be calculated as given by Kelley[20]

$$\Delta H_i(T) = A_i T + D_i T^2 + E_i + \underline{h}(T - T_{mi}) \cdot [B_i T + F_i - D_i T^2]; \quad i = \text{Sn, } NaClO_3\text{, NaCl} \tag{7}$$

$$\Delta H_i(T) = A_i T + B_i T^2 + D_i / T + E_i; \quad i = SnO_2 \tag{8}$$

$$\Delta H(T) = \sum_{i=products} \Delta H_i(T) - \sum_{i=reactants} \Delta H_i(T) \tag{9}$$

$$\underline{h}(T - T_m) \equiv \begin{cases} 0, & T < T_m \\ 1, & T > T_m \end{cases} \tag{10}$$

where $\underline{h}(T - T_m)$ is the step-function equal to zero for $T<T_m$ and $= 1$ for $T>T_m$. Heat capacity is the derivative of enthalpy with respect to temperature, and includes terms with both $\underline{h}$ and delta-function.

The industrially used samples (Figure 1) are manufactured from reactant powders and in the process of oxygen generation

Table 1. Parameters for ΔH (cal/mol) Calculation[20]

Species	A	B	D	E	F	T_m (K)	T_w (K)
Sn	4.42	2.88	0.00315	−1598	1072	505	3
SnO_2	17.66	0.0012	516000	−7103	—	—	—
$NaClO_3$	13.07	18.73	0.0185	−5542	672	528	7
NaCl	10.98	5.02	0.00195	−3447	3707	1073	8

the particles are heated rapidly.[4] There always exists a distribution in particle sizes and nonidealities (that is, defects and impurities) are present as well. Therefore, sample components melt in a temperature range close to T_m, rather than at a fixed temperature. This effect can be accounted for by replacing $\underline{h}(T - T_m)$ with a smoothed step-function, $g(T-T_m)$, with finite transition width T_w

$$\underline{g}(T - T_m) = \frac{1}{2}\left[1 + \tanh\left\{\frac{(T - T_m)}{T_w}\right\}\right] \tag{11}$$

Table 1 shows the values of melting intervals T_w, estimated from experimental TGA data for industrial samples. The heat capacity C_p exhibits sharp variations at temperatures close to melting points (Figure 2a). The enthalpy of reaction (Figure 2b) is also a function of temperature, since reactant heat capacities do not balance those of the products, and this feature was accounted for in the computations. It should be noted that melting may also affect heat-transfer rate in a porous sample by increasing contact area of powder particles. Because of lack of reliable experimental data on this effect, however, it was not included in the numerical simulations. The thermal diffusivity of the sample at low temperatures (300 to 500 K) was measured to be 0.003 cm^2/s.

Approaches Eq. 10 and 11 are consistent with each other. Test calculations were performed with half the melting intervals as compared to Table 1, and no significant effect of T_w on the resulting temperature and gas flow rate profiles was detected. Employing Eq. 11 is advantageous as it does not require extra boundary conditions for the melting region.

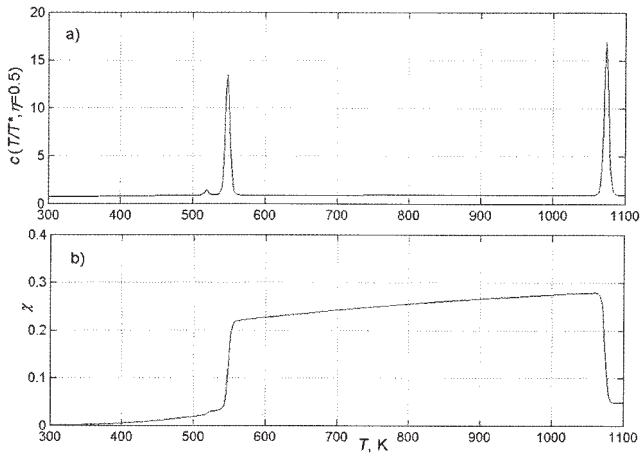

Figure 2. Temperature dependences of (a) heat capacity, and (b) reaction heat for a mixture of 10 mol % Sn, 45% $NaClO_3$, 45% NaCl.

The C_p and ΔH values are normalized by C_{p0} and $C_{p0}T^*$, respectively. The peaks in (a) correspond to tin (505 K), sodium chlorate (528 K) and sodium chloride (1073 K) melting.

Since in gas generators the reaction rate depends strongly on sample preheating by the flow, the variation of gas-to-solid heat-transfer coefficient $\tilde{\alpha}$ with flow rate was incorporated in the model. Because of direct proportionality of $\tilde{\alpha}$ and flow rate,[5] positive feedback may occur, where an increase in flow rate preheats the pellet more efficiently, enhancing combustion, which further stimulates gas release.

Estimates of the kinetic parameters in Eq. 6 were obtained using thermal analysis of typical oxygen generating mixtures and fitting a first-order rate expression to the experimental TGA curve. The X-ray analysis of quenched combustion wave[7] indicates that the two main chemical reactions in the mixture, $NaClO_3$ decomposition and Sn oxidation, are closely coupled: tin oxidation occurs within $NaClO_3$ conversion variation from ~20% to ~80%. This allows us to approximate the chemical evolution of the system using a single reaction rate expression. The activation energy value depends on the mixture composition and ranges from 80 to 130 kJ/mol for the mixtures studied.

It is convenient to operate with the product $V \cdot T_g$ rather than gas temperature. After rendering the equations dimensionless with parameters α, β and γ and characteristic values as defined in Notation, Eqs. 2 – 6 take the form

$$\frac{\partial v}{\partial x} = r(\eta, \theta) \tag{12}$$

$$\frac{\partial \psi}{\partial x} = \theta \cdot r(\eta, \theta) - \alpha_0 \cdot (\psi - v \cdot \theta) \tag{13}$$

$$\frac{\partial \eta}{\partial \tau} = r(\eta, \theta) \tag{14}$$

$$c(\eta, \theta)\frac{\partial \theta}{\partial \tau} = \frac{\partial^2 \theta}{\partial x^2} + (\beta + \chi(\theta)) \cdot r(\eta, \theta) + \alpha \cdot (\psi - v \cdot \theta) \tag{15}$$

$$r(\eta, \theta) = (1 - \eta)\exp\left(\gamma \cdot \left(1 - \frac{1}{\theta}\right)\right) \tag{16}$$

The boundary condition at the right end of the sample ($x = L$) was chosen as zero heat flux (Eq. 17), while two different cases were considered at the left (ignited) end, $z = 0$: zero heat flux through the sample (Eq. 18) or constant temperature (Eq. 19)

$$\left.\frac{\partial \theta}{\partial x}\right|_{x=L} = 0; \quad \tau > 0 \tag{17}$$

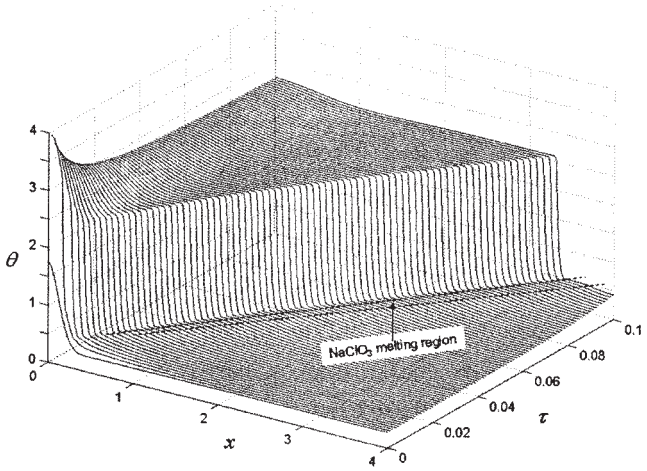

Figure 3. Consecutive temperature profiles ($\Delta\tau$ = 0.00125) during combustion wave propagation with significant convective heat transfer (α = 0.15, β = 2.35, γ = 14.33, θ_{ig} = 1.75, θ_0 = 0.2727, Δ_0 = 0.0075, boundary condition (Eq. 18).

The melting region occurs ahead of the combustion front, both moving from left to right.

$$\left.\frac{\partial\theta}{\partial x}\right|_{x=0} = 0; \quad \tau > 0 \tag{18}$$

or

$$\theta|_{x=0} = \theta_{ig}; \quad \tau > 0 \tag{19}$$

Since the left end of the generator is impervious to gas, we have

$$v|_{x=0} = \psi|_{x=0} = 0; \quad \tau \geq 0 \tag{20}$$

Initially, reaction conversion η is zero throughout the sample

$$\eta|_{\tau=0}; \quad 0 < x < L \tag{21}$$

The sample is ignited by an external heat source, which leads to the initial temperature distribution

$$\theta|_{\tau=0} = \theta_0 + (\theta_{ig} - \theta_0) \cdot \exp\left[-\frac{x^2}{4\Delta_0}\right]; \quad 0 < x < L \tag{22}$$

that arises from a specific heat input, determined by parameters θ_{ig} and Δ_0.

A time-explicit solver based on fourth-order derivatives was developed. The solver was tested following the guidelines given by Roache[21] and exhibited close to second-order convergence. The estimated numerical deviations did not exceed 0.1%, 0.4% and 0.5% for the combustion front position, gas flow rate and pellet-temperature distribution, respectively. For simplicity, a uniform spatial grid was used, which was refined until the computations revealed numerical convergence of the order 2 ± 0.2.

Results and Discussion

The model described earlier was used to simulate combustion wave propagation in media with phase transitions and convective heat transfer (that is, heat exchange between condensed core and the generated gas). The model was developed primarily to simulate combustion processes in oxygen generators, for which typical model parameters are known.[5] Some interesting features for cases involving high reaction heat values ($\beta \sim 2$) were observed and are also discussed below.

Reactant melting during combustion wave propagation is usually induced by heat conduction via the core and occurs in a melting front moving ahead of the combustion region. When the convective energy exchange is involved, as in this case, heat may be delivered by the flowing gas to the reactant core.

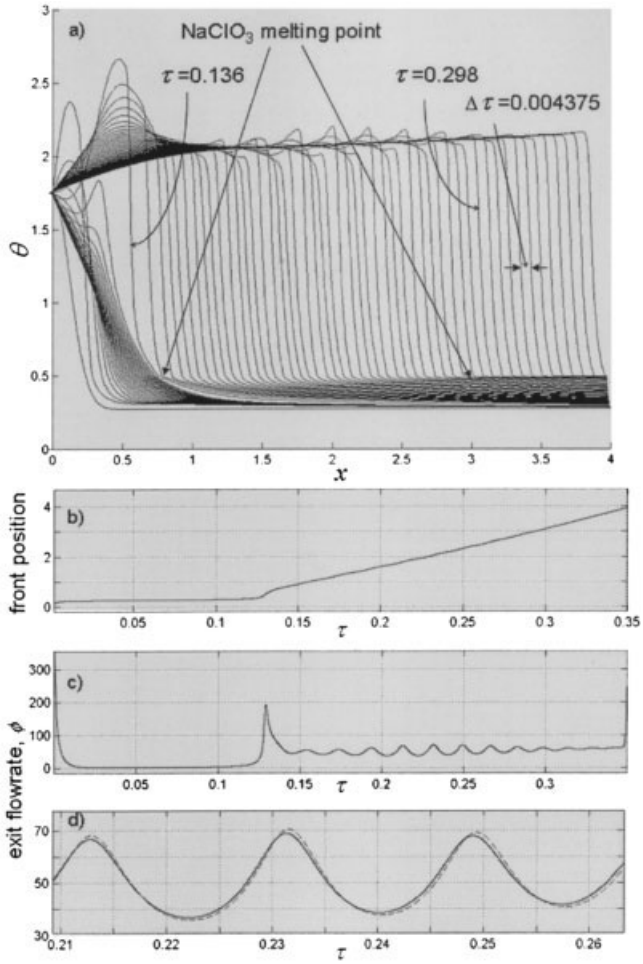

Figure 4. Combustion wave propagation computed for α = 0.0317, β = 2, γ = 14.33, θ_{ig} = 1.75, θ_0 = 0.2727, Δ_0 = 0.0075, boundary condition (Eq. 19).

(a) Consecutive core temperature profiles, (b) combustion front position (defined by η = 1/2); (c) exit gas flow rate evolution with time, and (d) effect of narrowing $NaClO_3$ melting temperature interval: the dashed curve represents simulations with T_w reduced by a factor of two.

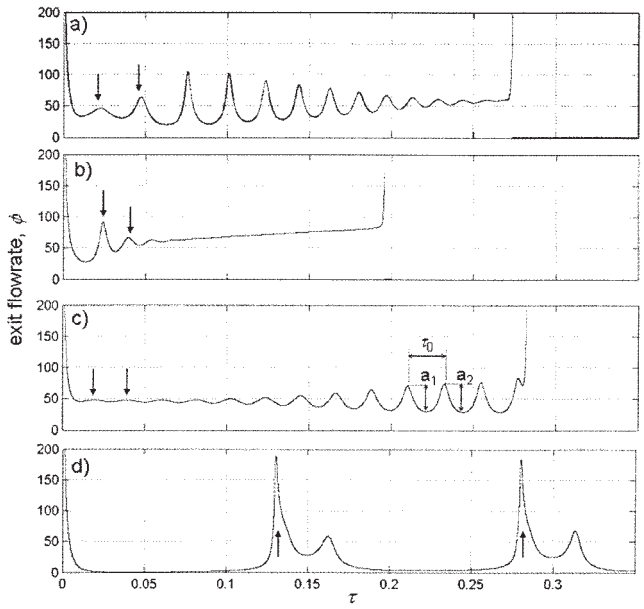

Figure 5. Gas generation for (a) both melting and convective heat transfer ($\alpha > 0$), (b) no melting of $NaClO_3$, (c) $\alpha = 0$ and no $NaClO_3$ melting, and (d) $\alpha = 0$ and $NaClO_3$ melts.

Unless otherwise specified, the calculations are made for the same parameter values as in Figure 4 and boundary condition (Eq. 18).

Thus, zero temperature gradient melting regions are allowed and melting is not necessarily confined to a narrow front.

An example of temperature profile evolution resulting from numerical integration of Eqs. 12 – 16 with boundary conditions (Eqs. 17, 18, and 20) is presented in Figure 3. It shows the growth of the melting region ahead of the reaction zone. With time, combustion front propagates along the sample, the generated gas preheats the core and the region of reactant melting becomes wider.

It is seen from Figure 4a – c that after an initial surge in the nearest vicinity of the left end, there exists a long induction period ($\tau \sim 0.13$) where a wider region is heated with essentially no reaction. Then, this region reacts quickly, resulting in rapid increase in temperature, front position and exit gas flow rate. Subsequently, the combustion wave propagates with oscillations in maximum temperature and exit gas flow rate ($\tau \sim 0.15$–0.3), which are dampened when the core ahead of the reaction zone is heated above $NaClO_3$ melting temperature ($\theta \sim 0.5$). Narrowing the melting temperature interval T_w by a factor of 2 has little effect on combustion characteristics (Figure 4d).

The effects of reactant melting and convective heat transport on pulsations in gas generation are also shown in Figure 5. Figure 5a describes well-developed oscillations, whose amplitude decreases with time, similar to those seen in Figure 4c. In the case of Figure 5b, the oscillations are effectively dampened and front propagation is stable. Figure 5c shows initially small but increasing oscillations and, thus, unstable front propagation as it should be expected for large activation energy values.[1] Finally, Figure 5d demonstrates well-developed pulsations characterized by large spikes in gas generation with virtually no reaction occurring between them. Sodium chlorate melting in the reaction zone stimulates pulsations in front propagation (Figures 5a vs. 5b), while gas-to-core heat transfer (5a vs. 5d, 5b vs. 5c) enhances process stability. This relates well with stability of convective filtration combustion.[10] The sharp increase in reaction temperature occurs when combustion wave reaches the sample end because of the zero heat flux condition (Eq. 17), and this effect is discussed in detail elsewhere.[22]

To quantify the effect of different factors on combustion stability, oscillations growth rate ξ, defined as the growth rate of the logarithm of oscillations amplitude, is used. The amplitudes of the first two peaks (shown with thick arrows on Figures 5a–d) were considered for this purpose. For example, ξ is large positive in Figure 5a, large negative for Figure 5b, positive for Figure 5c and essentially equal to zero for Figure 5d. In the case of small deviations, unlike Figure 5d, $\xi = 0$ represents the stability limit for front propagation.

Increasing reaction heat effect (β) and convective heat transport (α) stabilize the combustion front, while reaction activa-

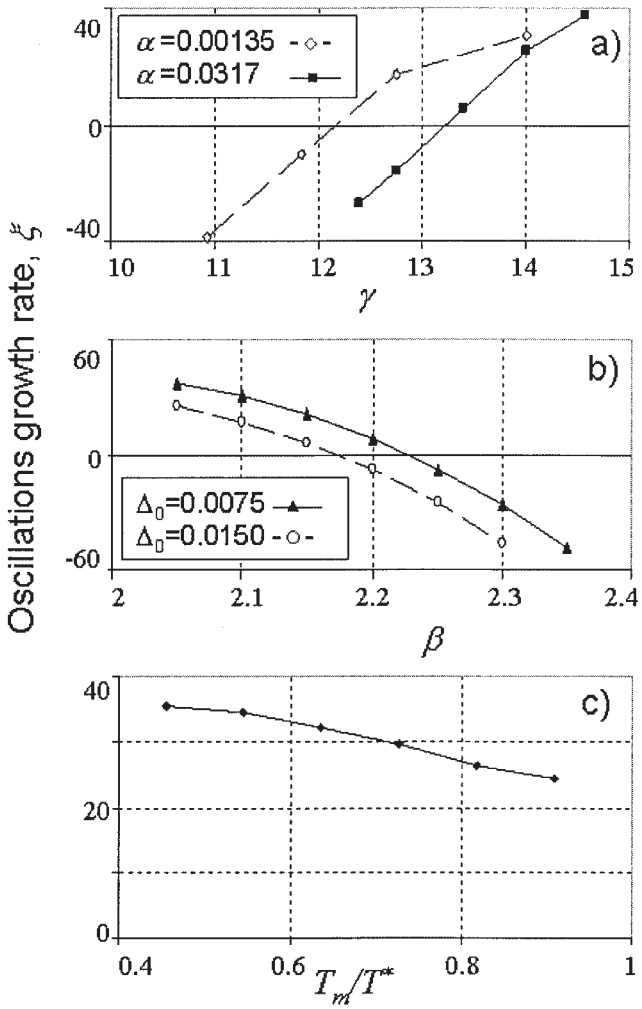

Figure 6. Effects on combustion stability of (a) activation energy and convective heat transfer, (b) reaction heat and initial heating, and (c) reactant melting temperature.

The parameter values, unless otherwise specified, are: $\alpha = 0.0317$, $\beta = 2$, $\gamma = 14.33$, $\theta_{ig} = 1.75$, $\theta_0 = 0.2727$, $\Delta_0 = 0.0075$, boundary condition (Eq. 18).

tion energy (γ) stimulates occurrence of pulsations (Figure 6). Simulations with various values for reactant melting point (T_m) were carried out. The results demonstrate that T_m has little effect on front propagation stability (Figure 6c), which implies that reactant melting destabilizes traveling combustion wave mainly by decreasing reaction heat effect (melting changes β by $\sim$0.2: see Figure 2b and Eq. 15).

Low exothermic mixtures ($\beta<0.7$) are used industrially for oxygen generation. As shown in Figures 7a and 7b, at low values of β, combustion exhibits pulsations similar to those discussed earlier (for example, Figure 4a). Taking z^* as the length of substantial (50%) variation in core temperature profile, typical dimensionless sample length (L) for which the experimental data are available,[4] is $\sim$80. A comparison of the numerical results for maximum core temperature (Figure 7c) with experimental values (Figure 7d) shows similar behavior. The oscillations in combustion temperature, defined as the maximum sample temperature at a given time, clearly indicate that the pulsations in front propagation are a significant factor in the experimentally observed instabilities.

It has been noted in the literature[9,17] that high melting temperatures stabilize combustion front propagation. This effect could be relevant to chemical oxygen generators as the experimentally measured maximum temperature is just below NaCl melting point. Figure 8 presents the results of numerical simulations, which demonstrate complete alleviation of pulsating instability by reaction product melting. The high temperature heat sink efficiently binds combustion temperature at NaCl melting point T_m, and this inhibits the occurrence of small deviations.

Conclusions

The stability of combustion wave propagation in chemical oxygen generators is analyzed numerically. The model includes detailed thermodynamic data, such as component melting characteristics and their heat capacity variation with temperature, along with kinetic parameters estimated from experimental data.

The formation of melting regions is demonstrated in cases with significant convective gas-to-core heat transfer. When the latter is involved, no condensed phase temperature gradient is required to heat the core, and this permits expansion of the thin melting front to a wide melting region.

It is shown that, by decreasing the effective heat of reaction, reactant melting is detrimental to combustion front stability. In accordance with prior theoretical results for simpler cases, the simulations demonstrate growth of pulsations with increasing reaction activation energy.

Numerical calculations also show a strong stabilization of front propagation when combustion temperature reaches the melting point of reaction product.

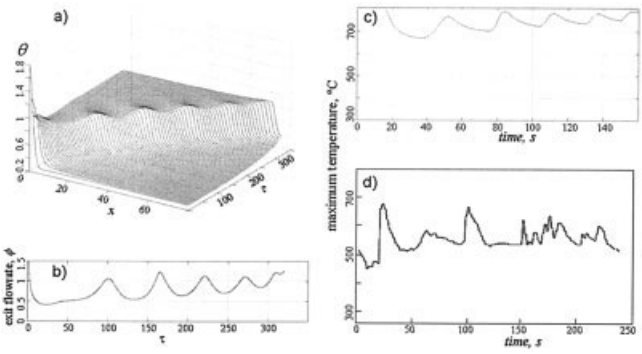

Figure 7. Low exothermic case pulsations: $\alpha = 0.005$, $\beta = 0.52$, $\gamma = 8$, $\theta_{ig} = 1.75$, $\theta_0 = 0.2727$, $\Delta_0 = 1.5$, boundary condition (Eq. 18).

(a) Consecutive temperature profiles ($\Delta\tau = 4$), (b) exit gas flow rate, and (c) maximum temperature variation with time ($t^* = 0.5$ s). The curve shown in (d) represents experimentally measured values (Figure 6a in Shafirovich et al).[4]

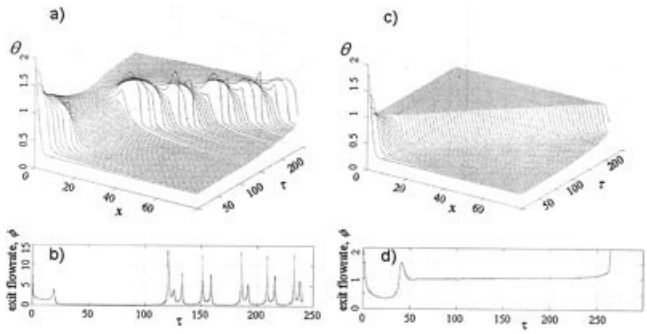

Figure 8. Stabilizing effect of product melting.

$\alpha = 0.0035$, $\beta = 0.71$, $\gamma = 11.16$, $\theta_{ig} = 1.75$, $\theta_0 = 0.2727$, $\Delta_0 = 1.5$, $\Delta\tau = 4$, boundary condition (Eq. 18). Temperature profiles (a, c) and exit flow rate (b, d) evolution for cases with (c, d) and without (a, b) NaCl melting, respectively. In the no-melting case calculations, T_m for NaCl was artificially set to 2000 K.

Acknowledgments

Acknowledgment is made to the donors of the Petroleum Research Fund, administered by the American Chemical Society, for supporting this research. We also thank R. Taylor and H. Groot (TPRL, Inc.) for thermal diffusivity measurements, as well as B. Seplyarskii (Russian Academy of Sciences) and C. Zhou (University of Notre Dame) for assistance in the early stage of this work.

Notation

$c(\eta, \theta) = C_p/C_{p0}$ = dimensionless heat capacity
C_p = condensed phase heat capacity, J/(mol · K)
C_{p0} = core heat capacity at 298 K, J/(mol · K)
C_{pg} = gas (that is, oxygen) heat capacity = 32 J/(mol · K)
d = annular space width in oxygen generators, typically 0.5 cm
E_a = activation energy, J/mol
$\Delta H(T)$ = temperature correction to reaction heat effect, defined in Eqs. 7 –11
$(-\Delta H_0)$ = standard reaction heat effect, J/mol
$(-\Delta H_r) = (-\Delta H_0) + \Delta H(T)$ = reaction heat effect, J/mol
k = condensed phase thermal conductivity, W/(m · K)
k_o = preexponential in reaction rate expression (Eq. 6), 1/s
l = sample length, typically 15 cm
$L = l/z^*$ = dimensionless sample length
$r(\eta, \theta) = R(\eta, T) \cdot t^*/\rho_0$ = dimensionless reaction rate
$R(\eta, T)$ = reaction rate, mol/(s · m^3), defined by Eq. 6
R_d = cylindrical core radius, typically 2.5 cm
R_g = universal gas constant, 8.31 J/(mol · K)

S = specific interphase surface area per unit core volume, 1/m; for gas flowing on the shell side of a cylindrical core $S = 2/R_d$
t = time, s
$t^* = k_0^{-1}e^{\gamma}$ = characteristic reaction time, s
T = core temperature, K
T_g = gas temperature, K
T_m = melting temperature, K
T_w = the width of melting interval, given in Table 1 and used in Eq. (11), K
T^* = characteristic temperature, 1100 K, the typical experimental combustion temperature[4]
$V^* = (3/2)z^*(\rho_0/t^*)$ = characteristic gas flow rate, mol/(s · m^2)
V = gas flow rate per unit core area, mol/(s · m^2)
$\nu = V/V^*$ = dimensionless flow rate
$x = z/z^*$ = dimensionless coordinate
z = coordinate along the sample, m
$z^* = \sqrt{k \cdot t^*/\rho_0 C_{p0}}$ = characteristic length, m

Greek letters

$\hat{\alpha} = \tilde{\alpha}/V$ = molar interphase heat-transfer coefficient, J/(mol · K).
$\tilde{\alpha}$ = interphase heat-transfer coefficient, W/(m^2·K)
$\alpha_0 = \hat{\alpha} \cdot S \cdot z^*/C_{pg}$ = coefficient in Eq. 13
$\alpha = (3/2)(\hat{\alpha} \cdot S \cdot z^*/C_{p0})$ = coefficient in Eq. 15
$\beta = (-\Delta H_0)/C_{p0}T^*$ = dimensionless reaction heat parameter in Eq. 15
$\gamma = E_a/R_gT^*$ = dimensionless activation energy parameter in Eq. 16
Δ_o = parameter in Eq. 22
η = reaction conversion
$\theta = T/T^*$ = dimensionless temperature
θ_o = dimensionless initial temperature of the sample
θ_{ig} = dimensionless initial temperature upon ignition Eq. 22
$\xi = [\ln(a_2/a_1)/\tau_0]$ = oscillations growth rate; a_1, a_2 and τ_0 are defined as shown in Figure 5c
ρ_o = initial reactant concentration, mol/m^3
$\tau = t/t^*$ = dimensionless time
$\phi = (2/3) \cdot [R_d^2/(R_d + d)^2 - R_d^2] \cdot v = 1.51 \cdot v$ = dimensionless exit flow rate
$\chi(\theta) = \Delta H(T)/C_{p0}T^*$ = temperature correction for β
$\psi = (V \cdot T_g/V^* \cdot T^*)$ = dimensionless gas enthalpy flow

Literature Cited

1. Novozhilov BV. Non-linear SHS phenomena: experiment, theory, numerical modeling. *Pure & Appl Chem*. 1992;64:955-964.
2. Merzhanov AG, Borovinskaya IP. Self-propagating high-temperature synthesis of refractory inorganic compounds. *Doklady Chemistry*. 1972;204**:**429-432.
3. Varma A, Rogachev AS, Mukasyan AS, Hwang S. Combustion synthesis of advanced materials. *Advances in Chem Eng*. 1998;24:79-224.
4. Shafirovich E, Mukasyan AS, Varma A, Kshirsagar G, Zhang Y, Cannon JC. Mechanism of combustion in low-exothermic mixtures of sodium chlorate and metal fuel. *Combustion and Flame*. 2002;128: 133-144.
5. Gusachenko LK, Zarko VE, Rychkov AD, Shokina NYu. Filtration combustion of an energetic material in a cocurrent flow of its combustion products: critical combustion conditions. *Combustion, Explosion, and Shock Waves*. 2003;39:694-700.
6. Aldushin AP, Rumanov IE, Matkowsky BJ. Maximal energy accumulation in a superadiabatic filtration combustion wave. *Combustion and Flame*. 1999;118:76-90.
7. Shafirovich E, Zhou C, Mukasyan AS, Varma A, Kshirsagar G, Zhang Y, Cannon JC. Combustion fluctuations in low-exothermic condensed systems for emergency oxygen generation. *Combustion and Flame*. 2003;135:557-561.
8. Aldushin AP, Matkowsky BJ, Shkadinsky KG, Shkadinskaya GV, Volpert VA. Combustion of porous samples with melting and flow of reactants. *Combust. Sci. and Tech.* 1994; 99:313-343.
9. Raymond CS, Volpert VA. Stability of uniformly propagating SHS waves in porous solids with melting and flow of reactants. *Chem Eng Sci*. 1996;51:4443-4462.
10. Aldushin AP. Heat transfer and convection combustion regimes of porous systems with filtration of heat carrier. *Fizika Goreniya i Vzryva*. 1990; 26:60-68.
11. Vakulenko S, Volpert V. Generalized travelling waves for perturbed monotone reaction-diffusion systems. *Nonlinear Analysis*. 2001;46: 757-776.
12. Beck JM, Volpert VA. Nonlinear dynamics in a simple model of solid flame microstructure. *Physica D: Nonlinear Phenomena*. 2003a;182: 86-102.
13. Beck JM, Volpert VA. A simple model of two-dimensional solid flame microstructure. *Combust Theory Modeling*. 2003b;7:795-812.
14. Krishenik PM, Shkadinskii KG. High-temperature thermal front in a medium with nonlinear thermal conductivity. *Doklady Physics*. 2003; 48:559-564.
15. Buckmaster J, Clavin P, Liñán A, Matalon M, Peters N, Sivashinsky G, Williams FA. Combustion theory and modeling. *Proceedings of the Combustion Institute.* 2005;30:1-19.
16. Shkadinskii KG, Khaikin BI, Merzhanov AG. Propagation of a pulsating exothermic reaction front in the condensed phase. *Fizika Goreniya i Vzryva*. 1970;1:19-28.
17. Gatica JE, Dimitriou PA, Puszynski JA, Hlavacek V. Melting effects on reaction front propagation in gasless combustion. *Intl J of Self-Propagating High-Temperature Synthesis*. 1995;4:123-136.
18. Raymond CS, Bayliss A, Matkowsky BJ, Volpert VA. Transition to chaos in condensed phase combustion with reactant melting. *Intl J of Self-Propagating High-Temperature Synthesis*. 2001;10:133-149.
19. Maglia F, Anselmi-Tamburini U, Gennari S, Spinolo G. Computer simulation approach to the chemical mechanisms of self-propagating high-temperature reactions: effect of phase transitions on the thermite reaction between O_2 gas and Zr powders. *J Phys Chem B*. 2002;106: 6121-6128.
20. Kelley KK. ed. Contributions to the data on theoretical metallurgy: high-temperature heat-content, heat-capacity, and entropy data for inorganic compounds. Government Printing Office; 1949.
21. Roache PJ. *Verification and Validation in Computational Science and Engineering*. Albuquerque, New Mexico: Hermosa Publishers; 1998.
22. Varma A, Cao G, Morbidelli M. Self-propagating solid-solid noncatalytic reactions in finite pellets. *AIChE J*. 1990;36:1032-1038.

Manuscript received Jun. 2, 2005, and revision received Sept. 27, 2005.